Ionics (2014) 20:1267–1273
DOI 10.1007/s11581-014-1082-7

ORIGINAL PAPER

X-ray structure refinement, vibrational spectroscopy, and ionic conductivity of $Na_{0.11}Ca_{9.64}Sm_{0.23}(PO_4)_6F_2$

M. Boujelbene · T. Mhiri

Received: 24 September 2013 / Revised: 29 January 2014 / Accepted: 30 January 2014 / Published online: 7 March 2014

Abstract The present paper is interested in the study of compounds from the apatite family, which is an apatite structure of individual rare earth substituted fluorapatite. In fact, an Sm-Bearing fluorapatite $Ca_{10-2y}Na_ySm_y(PO_4)_6A_2$ with x=0.11 and y=0.23 has been synthesized by solid-state reaction and characterized by X-ray powder diffraction. The site occupancies of substituents are 0.01091 for Sm and 0.02601 for Na in the Ca(1) position and 0.05317 for Sm in the Ca(2) position. Besides, the observed frequencies in the Raman and infrared spectra were explained and discussed on the basis of unit cell group analyses and in comparison with fluorapatite and other fluorapatites. In addition to the proton conduction, the possibility of a Na^+ contribution to the conductivity in the high-temperature phase is proposed. The highest overall conductivity values were found at $\sigma_{475\ °C}=2.03\times10^{-5}$ S cm^{-1} and Ea=0.60 eV.

Keywords Fluorapatite · X-ray diffraction · Infrared spectroscopy · Raman spectroscopy · Impedance spectroscopy

Introduction

The structure of apatite $Ca_{10}(PO_4)_6A_2$ A=F, OH, Cl apatite in the space group $P6_3/m$ allows a wide range of cation and anion substitutions [1–16]. In fact, the two Ca positions have distinct stereochemistries (Ca(1), equipoint 4f, CaO_9 polyhedron, Ca(2), equipoint 6 h, CaO_6 (A polyhedron)) are able to accommodate a variety of univalent, divalent, and trivalent cations as substituents. Concerning the substitution of the trivalent samarium (rare earth elements), it is charge compensated in various ways as in the following example:

$$2Ca^{2+} = Na^+ + Sm^{3+};\ Ca_{10-2y}Na_ySm_y(PO_4)_6A_2.$$

What is worthwhile to note is that the structure role of rare earth in apatite is currently unclear. Actually, minor amounts appear to replace Ca on the smaller Ca(2) position. Moreover, lanthanum, which is a synthetic $Ca_4La_6(SiO_4)_6(OH)_2$, is reported to be randomly distributed on both Ca positions [10]. In $NaY_9(SiO_4)_6O_2$, while Y is ordered in the 6 h position [Ca(2)], it is disordered with Na in 4f [Ca(1)] [12].

The structure of Nd-substituted fluorapatite showed that 80 % of the Nd was partitioned into Ca_2, in general agreement with Hughes [13, 14].

The preference of individual rare earth among multiple Ca positions in minerals (site occupancy) has not been extensively studied because of the inability of conventional diffraction methods to distinguish among individual elements on multiple occupied sites. We have reproduced the rare earth contents of the natural apatites studied to emphasize the extent of this problem for natural samples.

In order to understand the charge carrier diffusion processes occurring in apatite, investigations on calcium apatite substituted by samarium and sodium were performed. This work aims to determine the effects of the substitution of monovalent and trivalent ions for lead on the ionic conduction and the structural behavior.

In order to get a better understanding of these puzzling effects, we undertook a systematic study of the apatite containing rare earth. This paper is devoted to the case of a compound based on samarium. The objective is the examination of vibrational Raman and infrared spectroscopy of $Na_{0.11}Ca_{9.6}Sm_{0.23}(PO_4)_6F_2$.

M. Boujelbene (✉) · T. Mhiri
Laboratory of the Physico-Chemistry of Solid States, University of Sfax, Road of Soukra km 4, Sfax 3071, Tunisia
e-mail: m_boujelbene2010@yahoo.fr

Experimental methods

The $Na_{0.11}Ca_{9.64}Sm_{0.23}(PO_4)_6F_2$ compound was obtained by the solid-state reaction of Sm_2O_3, $Ca_3(PO_4)_2$ (Cerac, 99.95 %), CaF_2, Na_2CO_3, and $(NH_4)_2HPO_4$ (Merck, 99 %). After grinding, the mixture was heated at 300 °C for 6 h to eliminate ammoniac. The resultant powder was subsequently heated at 700 °C for 12 h and then at 840 °C for 24 h with intermittent grinding.

$$0.055\ Na_2CO_3 + 0.115\ Sm_2O_3 + CaF_2 + 3.88\ Ca_3(PO_4)_2 + 0.24(NH_4)_2HPO_4 \rightarrow Na_{0.11}Ca_{9.64}Sm_{0.23}(PO_4)_6F_2 + Ca_3(PO_4)_2 + 0.055CO_2 + 0.48NH_3$$

X-ray powder diffraction (XRD) pattern was determined by means of a PANalytical X'Pert PRO MPD diffractometer equipped with a detector X'cellerator operating with a secondary monochromator and using a CuKα radiation source ($K\alpha_1$=0.15406 nm and $K\alpha_2$=0.15444 nm). The diffraction pattern was recorded under ambient atmosphere over an angular range of 5°–80° (2θ), with a step length of 0.033° (2θ).

The Fourier transform infrared (FT-IR) measurements were performed at room temperature, on a Perkin-Elmer FT-IR Paragon 1000 PC spectrometer over the 400– 4,000-cm^{-1} region, in a KBr pellet. Furthermore, Raman spectra were measured with a LABRAM HR800 triple monochromator at room temperature under a×50 LF objective microscope. An He–Ne ion laser operating at about 20 mW was used (on the sample) as an excitation source (514.5 nm), with a spectral steps of 3 cm^{-1}.

Electrical conductivity measurements of apatite materials were undertaken using the impedance method on an HP 4194A impedance meter between 200 and 600 °C with the signal frequency ranging from 5 Hz to 13 MHz. An applied voltage was fixed at 100 mV. Powder was pressed under 5 t/cm^2. Electrodes were prepared by painting platinum paste on both sides of the sintered pellet surfaces, which were then heated at 600 °C to ensure a good electrical contact.

Table 2 Bond lengths (Å) and selected angles (°) of $Na_{0.11}Ca_{9.64}Sm_{0.23}(PO_4)_6F_2$

Bond lengths (Å)		Angles (°)	
M(1)–O(1)×6	2.412 (6)		
M(1)–O(2)×3	2.405 (3)		
M(2)–O(1)×3	2.248 (5)		
M(2)–O(2)×3	2.329 (7)	O(2)–P–O(3)×2	106.2 (4)
P–O(1)	1.471 (9)	O(1)–P–O(3)×2	116.7 (3)
P–O(2)	1.550 (7)	O(3)–P–O(3)	111.9 (3)
P–O(3)×2	1.503 (4)	O(1)–P–O(2)	107.80 (4)

Results and discussion

Refinement of the structure

The structures of the compounds in the solid are closely related to those of the common phosphate apatite, which have been frequently described in the literature [17]. They have been commonly determined by XRD using the Rietveld method refinement stating from the isostructural phase $Ca_{9.66}Na_{0.17}Sm_{0.17}(PO_4)_6Cl_2$ [18].

The final results of this refinement are presented in Table 1 (for the structure parameters and the R factors) and in Table 2 (for the atomic positions, selected bond lengths, and angles). Besides, Fig. 1 shows the observed, calculated, and different X-ray profiles of the powder diffraction of these apatite phosphates.

Discussion

The analysis of the tetrahedrons has revealed that the average P–O distance (1.506 (5) Å) is slightly shorter than the average values observed in fluorapatite (1.535 Å) [19]. The angles O–P–O are, on the other hand, seen to vary between 106.2° and 116.7°, with an average value (109.76°), which is very close to the one of a uniform tetrahedron (109.47°) (Fig. 2).

Table 1 Refined structure parameters and *R* factors from powder X-ray Rietveld analysis in P63/m space group of $Na_{0.11}Ca_{9.64}Sm_{0.23}(PO_4)_6F_2$

Atom	SOF	*X*	*Y*	*Z*	β (Å)
Na1	0.02601 (2)	0.66901 (16)	1/3	0.00255 (4)	0.30901 (8)
Ca1	0.89781 (2)	0.66901 (16)	1/3	0.00255 (4)	0.26785 (8)
Sm1	0.01091 (2)	0.66901 (16)	1/3	0.00255 (4)	0.30901 (2)
Ca2	0.94683 (2)	0.00557 (2)	0.258914 (14)	1/4	0.24274 (2)
Sm2	0.05317 (2)	0.00557 (2)	0.258914 (14)	1/4	0.28390 (5)
P1	1.00	0.37447 (2)	0.40634 (2)	1/4	0.69705 (6)
O1	1.00	0.49046 (5)	0.34392 (5)	1/4	0.82513 (5)
O2	1.000	0.46474 (5)	0.59701 (5)	1/4	0.82513 (5)
O3	1.000	0.27769 (5)	0.352 (5)	0.06435 (6)	0.82513 (5)
F	0.50	0.0000	0.0000	0.44087 (5)	0.66764 (8)

Conventional Rietveld factor Rp=14.9, Rwp=13.9, and χ2=1.561

Reliability factors for point with Bragg contribution *R* factors 2.77

SOF separated oscillatory fields

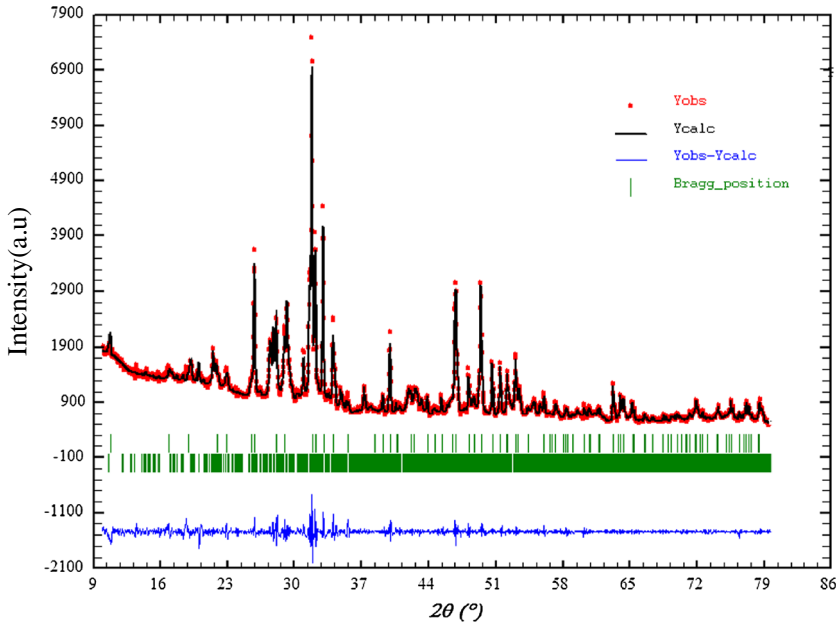

Fig. 1 The final Rietveld refinement plot of the $Na_{0.11}Ca_{9.64}Sm_{0.23}(PO_4)_6F_2$. *Points* correspond to the experimental values and the continuous lines; the calculated *pattern* and *vertical bars* indicate the positions of Bragg peaks. The *bottom trace* depicts the difference between the experimental and the calculated intensity values

There are two symmetrically nonequivalent M(1) and M(2) in the structure of $Na_{0.11}Ca_{9.64}Sm_{0.23}(PO_4)_6F_2$. The cations M(1) are coordinated to nine oxygen anions belonging to six distinct tetrahedrons. Each polyhedron is linked to four PO_4 tetrahedrons via corners and two other tetrahedrons via edges. The M(2) cations are inserted into fivefold sites that constitute the walls of the tunnels. Each polyhedron is linked to three PO_4 tetrahedrons via corners.

In the case of the M(1)–O distances, the nine distances have an average value of 2.409 (5) Å, which is quite similar to fluorapatite (2.56 (20) Å) (Fig. 3) [20]. In the case of the M(2)–O distances, on the other hand, the distance average value is 2.288 (4) Å, which is slightly smaller than the one observed in calcium fluorapatite 2.44 (13) Å (Fig. 4).

Therefore, the analysis of the final adjustments carried out for the observed and calculated diagrams indicates that there are three nonindexed lines that could be identified as minor impurities β-$Ca_3(PO_4)_2$.

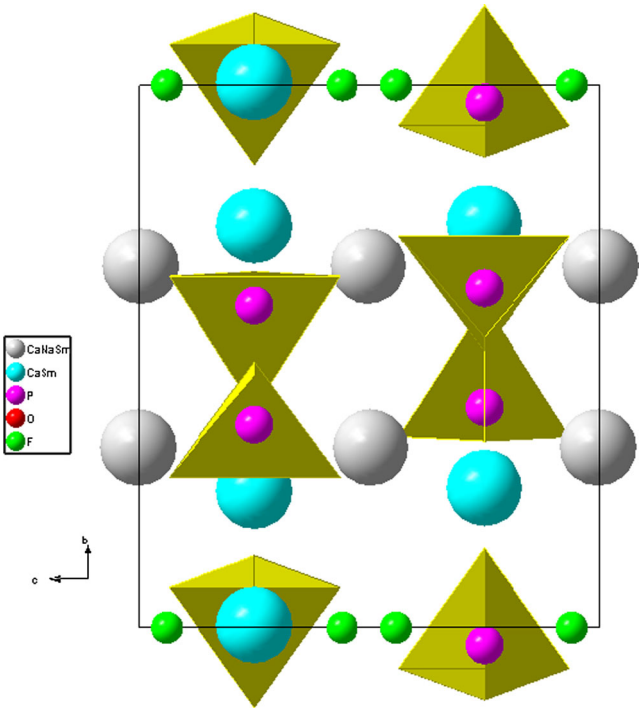

Fig. 2 Perspective view of $Na_{0.11}Ca_{9.64}Sm_{0.23}(PO_4)_6F_2$

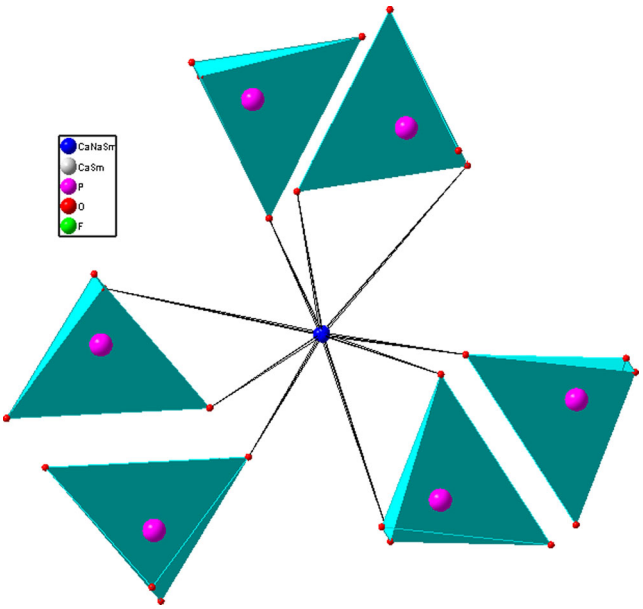

Fig. 3 Coordination of the metal in site (4f)

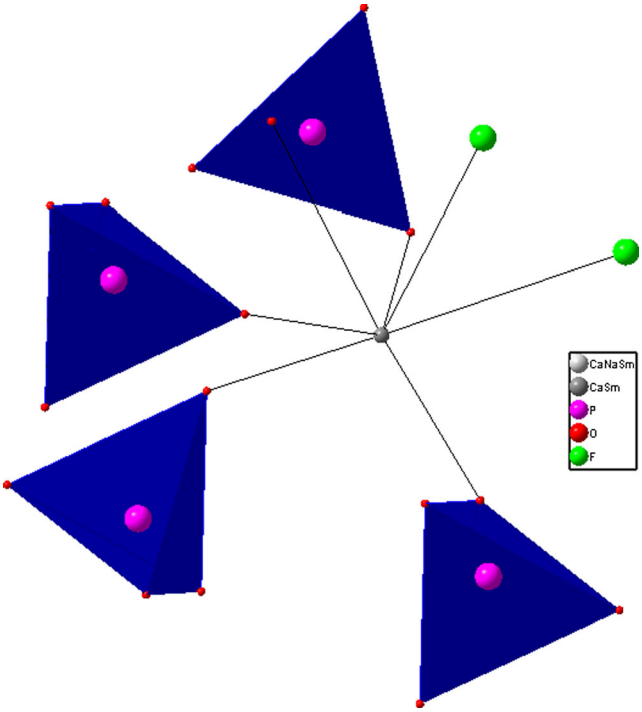

Fig. 4 Coordination of the metal in site (6 h)

Spectroscopy analysis

The IR and Raman spectra are shown in Figs. 5 and 6, respectively. The spectral data and proposed vibrational assignment are listed in Tables 3 and 4.

As shown in the Raman spectrum presented in Fig. 5, one strong band at 962 cm^{-1} was observed, which can be attributed to ν_1 (PO_4). The position of the band at 960 cm^{-1} is similar to the one previously reported by A. Hadrich [21].

The weaker peaks observed at 1,000 and 1,027 cm^{-1} and those recorded at 548, 558, and 575 can be accredited to the asymmetric stretching ν_3 and the asymmetric bending modes ν_4 of PO_4 groups, respectively. The bands assigned to ν_3

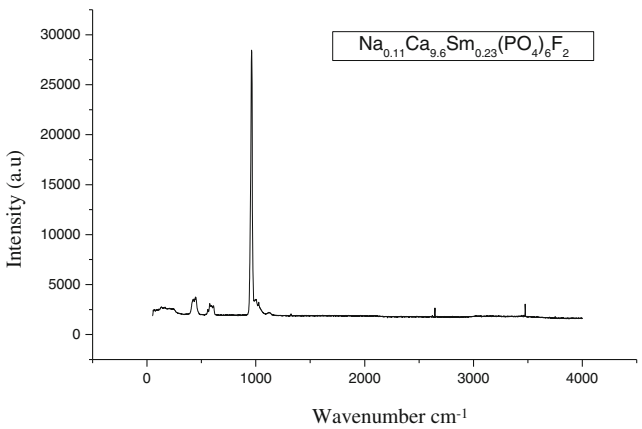

Fig. 5 Raman spectrum of $Na_{0.11}Ca_{9.64}Sm_{0.23}(PO_4)_6F_2$

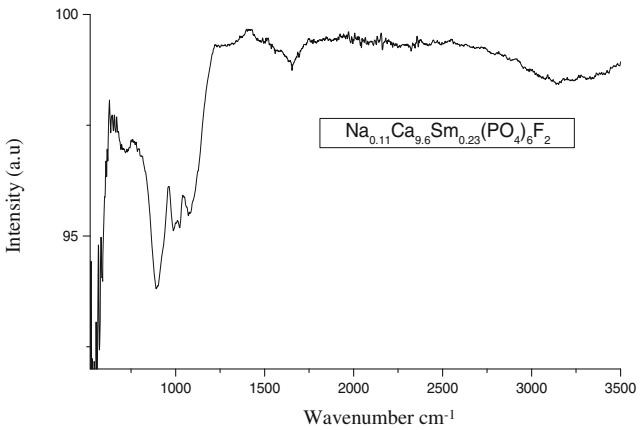

Fig. 6 Infrared spectrum of $Na_{0.11}Ca_{9.64}Sm_{0.23}(PO_4)_6F_2$

(PO_4) vibrations are reported at 1,000 cm^{-1}, whereas those assigned to ν_4 (PO_4), vibrations are described at 610 and 615 cm^{-1} for fluorapatites [21]. Regarding the weak lines observed at 421, 440, and 447 cm^{-1}, they could be assigned to the symmetric bending ν_2 mode.

With respect to the IR spectrum of the compound shown in Fig. 6, it is similar to that of fluorapatites. While the bands corresponding to the asymmetric stretching ν_3 (PO_4) are located at 1,045 and 1,003 cm^{-1}, the symmetric stretching ν_1 (PO_4) mode is observed at 943 cm^{-1}, such a mode was previously reported at 947 cm^{-1} in $NaPb_9(PO_4)_6F(H_2O)_{0.33}$ [22] and 930 cm^{-1} in $Pb_{10}(PO_4)_6F_2$ [23].

With regard to the two strong lines located at 563 and 600 cm^{-1} and observed at 575/600 and at 545/575 cm^{-1} in $Pb_{10}(PO_4)_6F_2$ and $Ca_{10}(PO_4)_6F_2$ [23], respectively, they are attributed to the asymmetric bending (ν_4) modes of PO_4 groups. Concerning the very weak line observed at 453 cm^{-1}, it could be attributed to the symmetric bending ν_2 mode.

The most interesting feature is the existence of few lines with much weaker frequencies than that in Ca_{10} $(PO_4)_6F_2$. This can be attributed to the presence of much mass heavier ions. Actually, with regard to the huge mass of samarium with

Table 3 Experimental wave number (cm^{-1}) of the PO_4^{3-} tetrahedron vibration of $Na_{0.11}Ca_{9.64}Sm_{0.23}(PO_4)_6F_2$

Raman (cm^{-1})	Infrared (cm^{-1})	Assignments
421	453	ν_2
440	–	
447	–	
575	571	ν_4
610	585	
962	986	ν_1
1,000	1,003	ν_3
1,027	1,048	

Table 4 The external modes Raman of $Na_{0.11}Ca_{9.64}Sm_{0.23}(PO_4)_6F_2$ (ANCSPF), flourapatite (FAP), and $Ca_6Sm_2Na_2(PO_4)_6F_2$ (CSPF)

ANCSPF	FAP	CSPF [29]
57		53
65		61
73		
81		
89		
94	98	
104		
129		
134	138	
158		
164		
206		207
232	234	232
248	266	
317	310	311

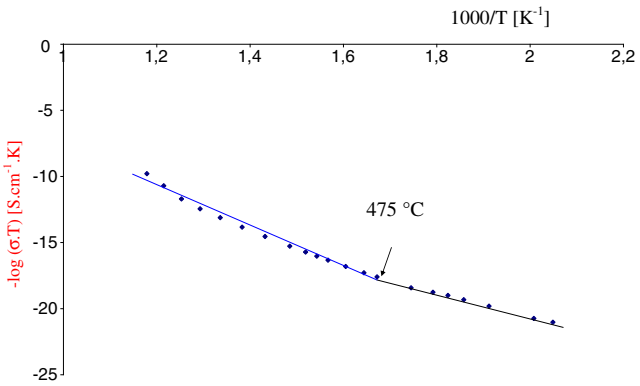

Fig. 8 Arrhenius plot log $(\sigma T)=f(10^3/T)$ of ionic conductivity for $Na_{0.11}Ca_{9.64}Sm_{0.23}(PO_4)_6F_2$

respect to the other components, several vibrations are presumably weakly coupled, and some modes can involve this ion alone. This is probably the case for two modes in the vicinity of 94 and 104 cm^{-1} since, with regard to the mass

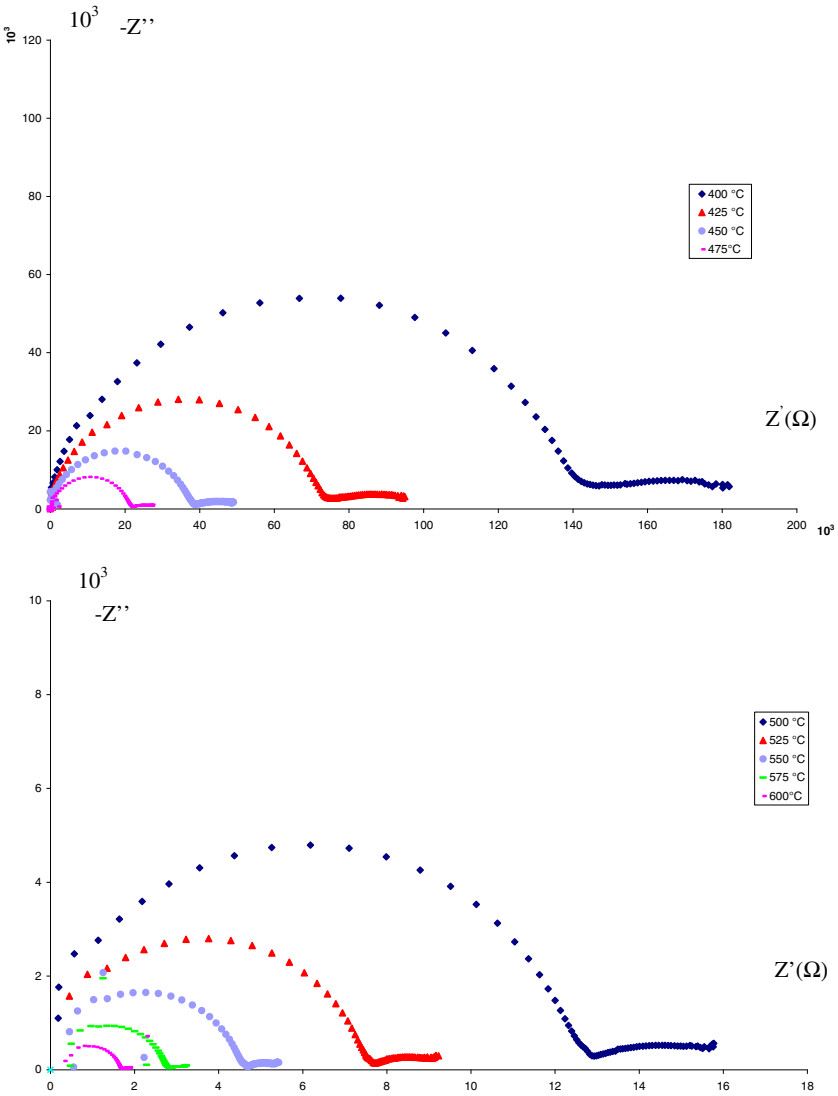

Fig. 7 Complex impedance diagrams of $Na_{0.11}Ca_{9.64}Sm_{0.23}(PO_4)_6F_2$ measured at various temperatures

Table 5 Comparison of electrical properties between fluorapatite and hydroxyapatite materials in relation with physical characteristics of M^{2+} ions

Compounds	Ca^{2+}	Ba^{2+}	Pb^{2+}
Fluorapatites	1.86	1.47	0.25
Activation energy Ea (eV)	1.36		
Hydroxyapatites	1.21	1.27	0.62
Activation energy Ea (eV)			
Activation energy Ea (eV)	0.6		1.6
$Na_{0.11}Ca_{9.64}Sm_{0.23}(PO_4)_6F_2$	1.3		

effect, they would correspond a vibration in the vicinity of 98 cm^{-1} in fluorapatite. The fact is that these modes appear with regard to the polarizability of the rare earth.

Conductivity data

The complex AC impedance responses of $Na_{0.11}Ca_{9.64}Sm_{0.23}(PO_4)_6F_2$ at different temperatures shown in Fig. 7 indicated the presence of two regions for measuring frequency. The high-frequency region might be due to the ionic conduction of mobile ions, including bulk and grain boundary, which collapse in the same semicircle. The low-frequency region, on the other hand, exhibited a conduction mechanism that could be related to the contribution of the electrode interface. The bulk and grain boundary semicircle that appeared at a high frequency was noted to get remarkably smaller at 600 °C. The sample impedance was generally observed to decrease with the increase in temperature.

The conductivity (σ) of $Na_{0.11}Ca_{9.64}Sm_{0.23}(PO_4)_6F_2$ was calculated using the following equation: $\sigma=(e/S)\times(1/R)$, where e, S, and R refer to the thickness, area, and resistance, respectively. The conductivity variation revealed an increase of conductivity with the rise in temperature, with a typical Arrhenius-type that indicated a semiconductor-like behavior having a linear dependence of electrical conductivity logarithm log (σT) on the inverse of temperature $10^3/TK^{-1}$ (Fig. 8). This temperature dependence of conductivity indicated that the electrical conduction in the material was a thermally activated process. It can be elucidated through the following expression: $\sigma=\sigma_0\exp(-\Delta Ea/kT)$, where σ, σ_0, ΔEa, k, and T refer to conductivity, pre-exponential factor, activation energy, Boltzmann constant, and absolute temperature, respectively.

The total activation energy was obtained as Et=0.6 eV for ionic hopping of mobile ions (Na^+ and F^-) along the c axis, including the bulk and grain boundary [24].

The conductivity of $Na_{0.11}Ca_{9.64}Sm_{0.23}(PO_4)_6F_2$ (2.3×10^{-5} S cm^{-1} at 475 °C) was relatively important than that of $Pb_{10}(PO_4)_6(OH)_2$ (2.05×10^{-7} S cm^{-1} at 500 °C) (Table 5) [25].

The break of Arrhenius lines at T=475 °C for the $Na_{0.11}Ca_{9.64}Sm_{0.23}(PO_4)_6F_2$ apatite is related to the pseudo ionic bond, which needs a high energy to romp this bound and to liberate the mobile ion (Na^+ or F^-; Fig. 8) [25–28].

The conduction mechanism is related to the translational hopping of sodium ions along the c axis of the unit cell from ordinary lattice sites in interstitial sites and back again, which are the only candidates for such a condition process.

Conclusions

The results from X-ray refinement have shown that the formula assigned to the new Sm-substituted Ca apatite was $Na_{0.11}Ca_{9.64}Sm_{0.23}(PO_4)_6F_2$. The analysis of data from vibrational spectroscopy has also provided support for the high symmetry $P6_3/m$ space group. This apatite contained channels where samarium ions are located in two different sites. Accordingly, further investigations that employed complex impedance were used to explore the possibility of cation conduction along these channels. The highest overall conductivity values were found at $\sigma_{475\ °C}=2.3\times10^{-5}$ S cm^{-1} and E_a=0.60 eV.

References

1. Nary Szabo S (1930) Z Kristallogr 75:387
2. Mehmel M (1930) Z Kristallogr 75:323
3. Kay MI, Young RA, Posner AS (1964) Nature 204:1050
4. Mackie PE, Elliott JC, Young RA (1972) Acta Crystallogr Sect B28: 1840
5. Elliott JC, Mackie PE, Young RA (1973) Science 180:1055
6. Sudarsanan K, Mackie PE, Young RA (1972) Mater Res Bull 7:1331
7. Hughes JM, Cameron M, Crowley KD (1989) Am Mineral 74:870
8. Hughes JM, Cameron M, Crowley KD (1990) Am Mineral 75:295
9. Hughson MR, Sen Gupta JG (1964) Am Mineral 49:937
10. Cockbain AG, Smith GV (1967) Mineral Mag 36:411
11. Mackie PE, Young RA (1973) J Appl Crystallogr 6:26
12. Gunawardance RP, Howie RA, Glasser FP (1982) Acta Crystallogr Sect B 38:1564
13. Hughes JM, Cameron M, Mariano AN (1991) Rare-earth-element ordering and structural variations in natural rare-earth-bearing apatites. Am Mineral 76:1165–1173
14. Fleet ME, Pan Y (1994) Site preference of Nd in fluorapatite [CalO(PO.),F,]. J Solid State Chem III:78–81
15. Suitch PR, Lacout JL, Hewat A, Young RA (1985) Acta Crystallogr Sect B41:173
16. Ronsbo JG (1989) Am Mineral 74:896
17. Hughes JM, Cameron M, Mariano AN (1991) Am Mineral 76:1165
18. Wyckoff RWG (1965) Crystal structures, vol 3, 2nd edn. Wiley, New York, p 228

19. Elliott JC (2002) Structure and chemistry of the apatites. Adv X-ray Anal 45:172
20. Fleet ME, Liu X-Y, Pan YM (2000) Am Mineral 85:1437
21. Hadrich A, Lautié A, Mhiri T (2001) Spectrochim Acta A 57:1673
22. Buvaneswari G, Varadaraju UV, Solid J (2000) State Chem 149:133
23. Laghzili A, Herch NEL, Bouhaouss A, Lorente G, Maquette J (2001) J Solid State Chem 156:57
24. Benmoussa H, Mikoua M, Bensaoud A, Bouhaouss A, Morineaux R (2000) Mater Res Bull 35:369
25. Tao SW, Irvine JTS (2000) Ionics 6:389–396
26. Laghzizil A, Barboux P, Bouhaouss A (2000) Solid State Ionics 128: 177
27. Naddari T, Feki HEL, Savariault JM, Salles P, Ben Salah A (2003) Solid State Ionics 158:157
28. Naddari T, Savariault JM, Feki HEL, Salles P, Ben Salah A (2002) J Solid State Chem 166:237
29. Toumi M, Smiri-Dogguy L, Bulou A (2000) J Solid State Chem 149: 308–313